Experimentally Matched Finite Element Modeling of Thermally Actuated SOI MEMS Micro-Grippers Using COMSOL Multiphysics

John V. Crosby and Mustafa G. Guvench*
University of Southern Maine
*Corresponding author: 123 John Mitchell Center, Gorham, ME 04038, guvench@usm.maine.edu

Abstract: Engineering MEMS devices using finite element analysis can be very rewarding, provided the analysis is valid, i.e. it accurately simulates reality throughout the desired range of input and resultant imposition upon dependent physical properties and behavior. With respect to FEM's use in MEMS, it is can be very useful. Doped single crystal silicon is a substance whose material and physical properties have been documented only sporadically, considering the infinitely many possible permutations of: 1) doping type, 2) concentration, and 3) doping profile; on top of these dramatic effects, two identical silicon devices, each at a different 4) temperature, can appear like two completely different materials: these four variables are what make using silicon for thermoelectric applications very difficult.

Here, to ensure future utility of FEM, we have compared experimental displacement data of two hot-arm-cold-arm microactuators of different sizes but very similar proportions to simulated parametric sweeps in order to extract the temperature coefficient of resistivity (TCR) and the surface-to-air heat transfer coefficient, commonly referred to as the convective heat transfer coefficient (CHTC). It is expected that 1) the temperature coefficient of resistance, would be the same or very close in both devices—since they are microfabricated by the same process on the same SOIMEMS wafers—and that 2) the heat transfer coefficient quantifying the surface-to-fluid heat loss would rise with increasing area, considering that the Grashof Number, the ratio of buoyancy force to viscosity forces, increases as the area normal to such forces increases. The experiment shows that parametric sweeps of such temperamental material yield somewhat problematic results. Of the two microactuators studied, the magnitude of the convective heat transfer coefficients were opposite than that expected: CHTC – large microgripper was 170/85 $W/m^2 \cdot °C$ (bottom and sides/top) and of the smaller one CHTC was 1200/600 $W/m^2 \cdot °C$. TCRs of the devices were within 50 % of one another, at least establishing a likely range for refinement of experimentation.

Keywords and Phrases: MEMS, Micro-actuators, Finite Element Modeling, Silicon, TCR, Heat Transfer Coefficient

1. Introduction

In "Micro-Electro-Mechanical-Systems" shortly known as MEMS, one of the most important and effective principles of creating transduction of electrical power to displacement force is thermal expansion. A slim beam of MEMS material, typically Silicon, is heated by the application of electrical current via electrical Joule heating; it expands and creates motion. In the design of many MEMS devices this method of transduction is preferred because of the orders of magnitude larger forces it can create in comparison with the forces created with the ubiquitous electrostatic comb drives. Therefore it is generally employed in microactuator and micromanipulator designs like MEMS microgrippers. Relatively large forces created by thermal expansion can lend themselves to amplification of the resulting small displacements via lever or bimorph action. Calculation or prediction of displacement and forces created by the strongly coupled sequence of terminal voltage => current distribution => uneven joule heating => heat transfer => temperature distribution => temperature dependent electro-mechanical-thermal properties of materials and heat losses => thermal expansion => stress distribution when coupled to three dimensional geometric effects becomes almost impossible except with a finite element tool. COMSOL Multiphysics and its MEMS module have proven to be the right tool for such a problem.

Indeed, engineering MEMS devices using finite element analysis can be very rewarding, provided the analysis is valid, i.e. it accurately simulates reality throughout the desired range of input and resultant imposed physical properties

and behavior. Doped single crystal silicon, though, is a substance whose material and physical properties have been documented only sporadically, considering the infinitely many possible permutations of doping type, concentration and profile. On top of those dramatic effects, two identical silicon devices, each at a different temperature, can appear like two devices made of completely different material. Those four variables are what make using silicon for thermoelectric applications very difficult.

Here, we have compared experimental displacement data of two different hot-arm-cold-arm microactuators, each of a different size, to simulated parametric sweeps to extract the likely temperature coefficient of resistivity (TCR) and the surface-to-air heat transfer coefficient, commonly referred to as the convective heat transfer coefficient (CHTC).

2. Device Analysis

2.1 Device Overview

The ruling mechanisms of our devices are joule heating and thermal expansion of the device, a cantilever-type single-crystal silicon structure. The potential is to be supplied to the microgripper through bonding pads to which the functional arms are connected as it hovers above a fully open trench. In the narrow (hot) arm, dramatic heating occurs due to the n^{++} doped silicon's relatively low resistivity and the high resistance manifest in the narrowness of the cross section of the hot arm. This heat is then: 1) conducted from the n^{++} doped layer where it originates through the heater in all directions; 2) conducted to the air, which may become turbulent depending on the scale of action; and 3) radiated in all directions to any black or grey bodies in its path. The large mass on the wide arm facilitates the removal of heat through conduction and convection to the surrounding fluid, in this case, air. Since the large arm, with only a relatively short narrow section, stays cooler, it expands less; thus the entire freed and hanging section of the device, anchored at the substrate, tends to move in the plane, away from the narrow hot arm, toward the wide cold arm. That is, the device moves away from the source of the expansive forces until it reaches a steady-state equilibrium with elastic forces manifest in the narrow sections of both arms near where thy are fixed to the substrate.

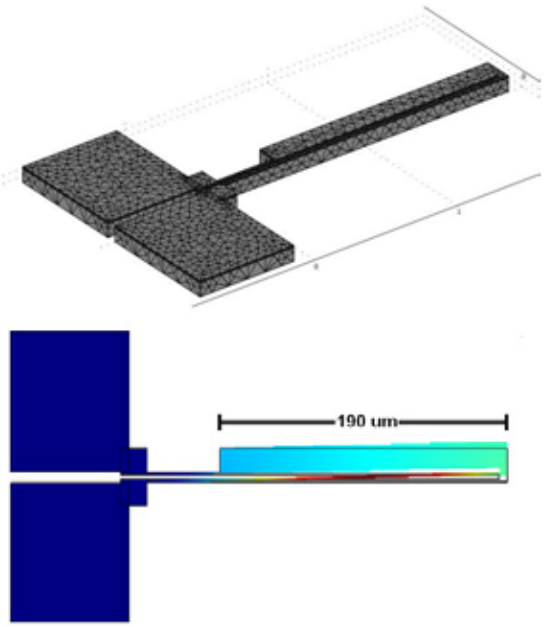

Figure 1 [top] A perspective view of the smaller of the two hot-arm-cold-arm microactuator devices, showing meshed geometry. [bottom] The top view of the same structure showing: 1) the dimensions, 2) the displacement due to thermal expansion, illustrated by the colored shape (the electrically excited device) being distorted outside of the black outline, the ambient temperature, un-excited shape, and 3) a temperature profile, where red is the hottest and blue is the coldest.

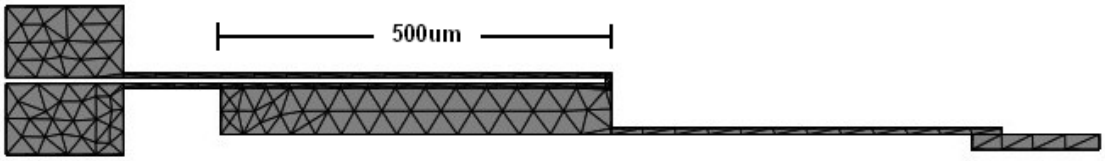

Figure 2: Meshed large microactuator structure. Only one arm is necessary to simulate the symmetric device, saving computer resources. The tweezer attached to the end of the actuator allows for higher precision in manual measurements of experimental displacements. Unfortunately, the smaller device, which has no attached tweezer, was designed and fabricated before there was any intention of performing this type of experiment.

2.2 Thermoelectric Microgripper Fabrication

The SOIMUMPs wafers are essentially two single crystal silicon wafers bonded back to back on their <100> plane. A 1µm oxide layer lies between the two wafers to insulate the device layer from the substrate. A thinner layer of oxide is deposited on the entire backside of the bottom wafer. The top wafer is etched to a thickness of 10µm, and then doped with phosphorus by annealing with phosphosilicate glass (PSG), a process forming the quintessential device layer or *field* silicon, leaving the 400µm *handle wafer* and its bottom-side insulating silicon oxide cover intact.

The SOIMUMPs process is a simple one. First, using standard photolithography, a pattern of pad metal consisting of 20nm of chromium (used for adhesion of silicon to gold) underneath 500nm of gold is deposited by e-beam evaporation for electrical contacts and connectivity. Once the finished pad metal is protected with photoresist, a DRIE etch of silicon is done for device features, often thermo-electromechanical in nature. The top layer is then covered in protective oxide while a trench is back-etched in three steps to release the device(s) above: (1) RIE removes the bottom oxide at the trench; (2) removal of the substrate using DRIE, stopping at the insulating middle oxide, and (3) a wet etch is used to remove the middle oxide from the bottom side of the field silicon. Once the trench is fully formed, the protective oxide is etched from the top surface. Next, a photoresist mask is placed on the device layer so a final blanket metal consisting of 50nm of chromium and 600nm of gold can be deposited for such things as residual stress, added mass, a second matrix of connectivity or any other function a designer can imagine.

Figure 3: A cross-section of a fixed-free type cantilever device (dimensions are not to scale). The n^{++} silicon is dark red, the n^{+} layer is red, the middle oxide is black, the substrate is blue, and the gold pad-metal is yellow.

The specifications of our designs are as follows. The 10µm thick active layer has been n^{++} doped to a depth of 1µm for an average sheet resistance of 20ohms/□ and the remaining, more lightly doped n-type device layer silicon below is 1ohm/□, both according manufacture specifications [1].

2.3 Electrothermal Properties

The joule heating (power loss), which takes place only in silicon where current density is significant, is mostly caused by electron-lattice collisions, and to a lesser extent, electron-electron collisions, both of which cause electrons to lose momentum. That decrease in momentum and thus electric potential energy, is manifest as an equal increase in kinetic energy, heat; and at higher temperatures, a sort of crowding occurs, leading to higher order temperature effects, a temperature dependent conductivity, described momentarily.

Joule heating is very much temperature and doping dependent for many reasons. First, doping increases the amount of charge carriers and establishes a majority carrier (provided $N_D \neq N_A$), a carrier type which is highly uncompensated in n^{++} silicon; accompanied by an electric field, doping simply provides more current, and thus, more collisions leading to higher temperatures at lower voltages; a higher temperature is simply an increase in frequency of collisions. From above, this increase in randomness of the electrons (as opposed to their momentum being only in the direction of the applied electric potential), an increase in kinetic energy—again, that decrease in the average momentum in the direction of the inducing potential—can be thought of as a decrease in mobility, an anisotropic vector, though most often expressed as a scalar average, as it will be here for engineering purposes. Electrical conductivity is a function of mobility, and is given by

$$\sigma = q\left(N_A \mu_p + N_D \mu_n\right) \quad (1)$$

where q is the value of a single charge, 1.61×10^{-19}, N_A is the number of acceptor atoms per cm^3 N_D is the number of donors per cm^3, μ_p is the

mobility of holes, and μ_n is the mobility of electrons. When $N_D >> N_A$ the equation can be simplified by simply omitting hole contribution, thus conductivity is simply given by the reasonable estimation

$$\sigma(N_D, T) = qN_D\mu_n(T) \quad (2)$$

Since current is proportional to mobility through ohms law and also from above, having established the theoretical mechanism for mobility decreasing with temperature, holding potential constant, we see a decrease in current flow with an increase in temperature. (The addition of charge carriers due to thermal excitement is many orders of magnitude less than the number present in such highly doped silicon, and is thus insignificant.) This is conveniently modeled as a very simple linearly temperature dependent resistance for many conductors but for silicon, the linearity is only an approximation, not a terribly bad one in our case as we shall see, but approximate just the same. The formula is

$$\rho(T) = \rho_0[1 + \alpha_R(T - T_0)] \quad (3)$$

where ρ_0 is the resistivity at a reference temperature, α_R is the temperature coefficient of resistivity (TCR), and T_0 is the reference temperature. Literature available on the subject of heavily doped single crystal silicon suggests that its resistivity changes only very slightly with temperatures up to 250°C [2 – 3]. Despite very slight exponential behavior [2], the linear model is used for simplicity, with α_R theoretically valued around .002°C^{-1} [2] and an initial value of ρ_0 at 2.0x10^{-5} Ω·m (calculated by multiplying SOIMUMP's specified sheet resistance by 1µm, the estimated thickness of the n^{++} doped layer field silicon, and later disconfirmed and replaced by a new value through analysis of I-V characteristics gleaned through a voltage sweep experiment with a prototypic device mentioned at length below).

2.4 Thermal Power Loss Considerations

For a silicon device this size submerged in air, radiation is consistently ignored at the temperature range of interest (20°C – 363°C) [5 – 12]. Nevertheless, rather dramatically divergent opinions—even those of researchers studying similarly sized devices [5]—exist as to the dominant heat loss mechanism. Even so, all research studied seems to concur that all heat transfer parameters are size dependent. Conduction to the substrate (essentially an infinite heat sink) is modeled to be the only mechanism in [5] and [6], conduction to substrate in parallel with conduction to the air in [7 – 9]. Researchers in [10 – 15] have modeled their design to include convection to the air and conduction to the substrate. In [16 – 18] convection, conduction, and radiation are all three taken to be significant, yet [18] studied a temperature range similar to that in which most cited have attested that radiation was insignificant. (It seems that inclusion of the indeed relatively insignificant radiation parameter comes down to preference of precision.) Indeed, in our preliminary examinations of the COMSOL® software, realistic radiation heat transfer coefficients caused only unrecognizable steady state temperature differences below 400°C. In general, with respect to the convection to the air, the size of the device determines its effect; in smaller devices the Grashof number, the ratio of the buoyancy forces to the viscous forces of air, becomes lower as size decreases, which rules out significant convection in such devices [7], [8], and [10]. (A substantial amount of attention will be given to this idea in this study; in fact one of its main goals is to confirm the size dependence of surface-to-air heat loss for the purpose of educated optimization of a resonating heater to be used to sense the presence of gas in high vacuums.)

The researchers who chose to analyze their models using conduction to air as the dominant heat transfer mechanism have done so conceding that a certain amount of power is dissipated through the surface of a heater device on the microscale. Mankame and Ananthasuresh [16] have attested to earlier accidental findings of ours that when no lumped heat transfer coefficient is applied as a surface boundary condition when simulating a powered hot-arm-cold-arm actuator such as ours, the displacement is in the opposite direction than that observed, even when the top area of the device is very small. This means that no matter what the heat transfer mechanism is, a certain amount of heat must be removed from the surface to represent

reality. Though Pike and Gardner [13] have suggested a second order effect of temperature to convective heat loss in devices this size, all others have simulated using a linear model.

In sum, concerning our design, it is difficult to determine exactly which heat loss mechanism to the air will dominate. We have opted for the use of a linear model using a lumped coefficient which will model the removal of heat from the air-exposed surface as a function of temperature, keeping in mind that there is no data available as of this paper to establish the amount of heat loss from the surface. This will be dealt with below as one of two main goals of the study.

The heat transfer due to convection (and/or conduction in our models) as a function of temperature is given by

$$q(T) = h(T - T_0) \quad (4)$$

where h is the convective heat transfer coefficient (CHTC), a lumped parameter with units W/m^2·°C, i.e. it represents the removal of constant power for every degree Celsius, T, in the form of heat per area per °C, an assumption of linearity that is not entirely valid, but which serves as a good approximation. Finally, T_0 is the temperature of the surrounding fluid, in this case, air.

[10 – 12] suggest that coefficients on the top surface will be twice as much as those on the bottom and sides—due to convection's effect being greater on surfaces whose normal vector is upward-vertical (opposing gravity)—so that paradigm is used here.

2.5 Thermal Conductivity Theory

Silicon, being a metalloid in group IV of the periodic table of elements, possessing a diamond shaped lattice, is affected by heat much differently than other materials; lattice vibrations are predominantly responsible for conductive heat transfer. Empirical thermal conductivity vs. temperature data for single crystal silicon has been established [19] and [20]. It has also long been confirmed that the thermal conductivity is negligibly dependent on doping at operating temperatures above -173°C [21]. Figure 4 shows an interpolated plot of thermal conductivity as a function of temperature. A least squares regression of available data [19] in the domain of interest yields a power-type function, $k(T) = 115598T^{-1.177}$, which is used in the simulation in place of a single valued coefficient in the thermal conductivity differential equation. The steady state equation then becomes

$$k(T)\nabla^2 T + Q = 0 \quad (5)$$

where Q is the power generated, in this case through joule heating [$Q = I^2\rho(T)L/wt$ where L/wt are the dimensions and $\rho(T)$ is the resistivity according to (3)].

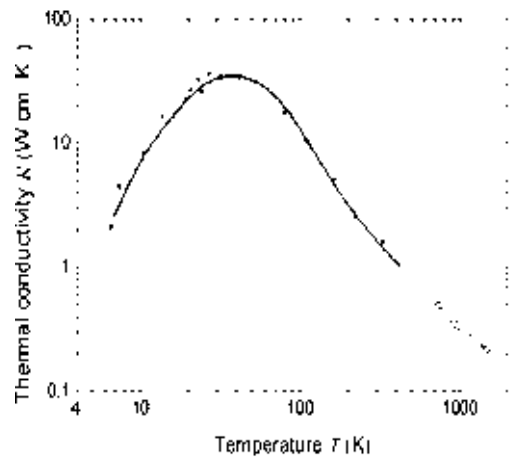

Figure 4: An interpolated curve from experimental data for single crystal silicon. Used by permission of Ioffe Physico-technical Institute at http://www.ioffe.ru/SVA/NSM/Semicond/index.html

The actual solution time will be increased to an extent, since $k(T)$ is a non-integer power function. Such a function takes more time to estimate numerically than simple multiplication in computer algorithms.

Due to this thermal conductivity being so predominant, the boundary conditions of the bottom side of the pads will be set to a constant temperature, modeling an infinite heat sink, a reasonable assumption.

2.6 Thermal Expansion

Thermal expansion of solids is most often modeled by

$$\alpha_E = \frac{\Delta L}{L_0 \cdot \Delta T} \quad (6)$$

where α_E is the linear thermal expansion coefficient, ΔL is the change in length from L_0, and ΔT is the change in temperature that causes the expansion. This is a simple equation; however, in the case of doped single crystal silicon, there is very little evidence to suggest that things are indeed this simple. In fact, from an experiment in [22], there is good evidence that pure single crystal silicon has a linear thermal expansion coefficient that increases dramatically from 25°C to 725°C: from 2.57 to 4.33 in that temperature range. However, we are not using pure silicon here, but instead highly doped silicon, which is inherently subject to residual stress from the doping process, i.e. interstitial and, to a lesser extent, substitutional atoms pushing outward on the lattice. To our knowledge, there have been no studies to show linear thermal expansion coefficient of single crystal silicon as a function of temperature *and* doping. This problem alone introduces much uncertainty into our study, uncertainty that can only be met with fairly informal assumptions when research is not forthcoming. Thus, for lack of anything better, we have opted to stick to the well-known ambient temperature value, 2.60 x 10^6 m/°C.

3. Use of COMSOL Multiphysics®

3.1 Introduction to Simulation

In order to isolate CHTC and TCR, it was essential to vary those parameters and compare them to experiments of the prototypic microactuators. To accomplish this, rather than manually varying each parameter and solving for each combination, an N^3 parametric sweep was done, [Voltage(TCR(CHTC))]. The intended displacement was in the plane of the device, toward the cold arm; post-solution, using COMSOL's parametric sweep function, having automatically saved each solution as its own file, it was a simple matter to open up each file and record the maximum displacement (as of the current version, v3.5a, there is no way to our knowledge of specifying to record the temperature at a certain, single point in the output text file generated by the parametric sweep. It appears that in that text file, one may include any dependent variable inherent in the application modes used, but the values are averages). Once the displacements from the appropriate values of voltage were lined up as a function of TCR and CHTC (voltage was not a variable to isolate. Experiment showed: 1) with the larger device, what voltage range the prototype could handle before making contact with the other side of the device and 2) with respect to the smaller device, at what temperature it would actually melt and completely disintegrate (as is what actually happened to the first of our several identically micromachined small microactuators).

3.2 Large Microgripper

First, the experiment was performed by placing the prototype under a microscope, probed at the two pads, where potential was stepped from one to seven volts. By analyzing the current vs. voltage at 1 volt, a good estimate of the reference resistivity, ρ_0, was gotten via ohms law, considering simply that resistance is proportional to resistivity multiplied by length and divided by the cross-sectional area of the conductor. By evaluating a point at the end of the hot arm in any one simulation, one can easily determine the voltage divider between the entire device and the hot arm. This way, the reference resistivity was found to be 6.45×10^{-6} Ω·m. The thicker, more lightly doped silicon was set at TCR = .002 W/m^2·°C with a reference conductivity of 1×10^2 S/m; since the conduction of this layer compared to the highly doped region was negligible, as long as it appeared to have a roughly positive TCR, then it would serve to not interfere with the realism of the simulation.

By the first sweep, using midpoints of both variable parameters gleaned from the literature, a rough estimate of CHTC = 240/120 W/m^2·°C and TCR = .005 °C^{-1} was arrived at by comparing experimental displacement of a prototype device to the many COMSOL generated voltage sweeps, each with a different combination of the CHTC and TCR. The least sum of the squares of the residuals was used for a best fit.

Next, since the first sweep had been wide and imprecise, a more refined parametric sweep was done using the above solutions as the midpoints, honing in with more detail at these values.

3.3 Small Microgripper

The reference resistivity from the first large microactuator was compared to the reference resistivity of the second, small microactuator. They were determined to be within 1% of one another, thus, in the simulation, $\rho_0 = 6.45\text{x}10^{-6}$ $\Omega\cdot$m was entered as the appropriate subdomain condition in the n^{++} silicon. An initial parametric sweep of the small microactuator was undertaken to establish the vicinity of functional values (as in above), upon which time a second, more refined sweep honed in on the final results.

4. Results and Discussion

With respect to the large microactuator, the final parametric sweep showed the effective TCR and the CHTC to be .005 °C^{-1} and 85/170 W/m$^2\cdot$°C respectively. Unfortunately, the effective values of CHTC of the second, smaller microactuator were opposite to that expected: CHTC = 600/1200 W/m$^2\cdot$°C. The results for TCR, though not 'opposite' of that expected, are cause for concern: TCR = .003 °C^{-1} is -25% different than their average, .004 °C^{-1}.

It was expected that convection in the air surrounding the small device would facilitate cooling less due to viscosity overcoming the buoyancy at the smaller dimensions. This may very well have been the case; however, this phenomenon may have "backfired" in that on the top of the device it was not significant enough to outdo the heat conduction to the substrate through the air underneath, which moved less due to it's small Grashof number in the much smaller trench, i.e. the air in the trench stayed stationary enough to conduct much heat back to the substrate, not only being able to lose more heat but also decreasing the temperature gradient between the arms and the substrate.

An important thing to note is the lack of data available on the thermal expansion of silicon as a function of temperature and doping concentration. In order to really isolate these variables, a comprehensive study of doped silicon's thermal expansion using the methods in [22] will yield sufficient data to account for the thermal expansion, an obviously under-represented degree of freedom of the microactuators in this experiment. Also, Lee et al in [7] warned of heat loss to the substrate depending on things such as whether or not the membrane (cantilever in our case) was fully backside released or just deeply etched leaving no through-hole. In a future experiment, such considerations need to overcome some of the oversimplified assumptions of this experiment. This will lead to better understanding of heat loss as a function of shape and size, decidedly, even by this experiment, a quintessential factor.

4.1 Large Microactuator

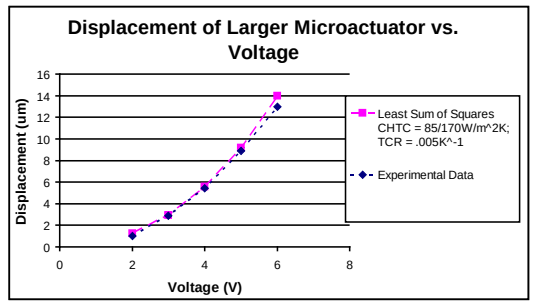

Figure 5: Results of the best-fit large microactuator sweep plotted with the experimental displacement vs. voltage.

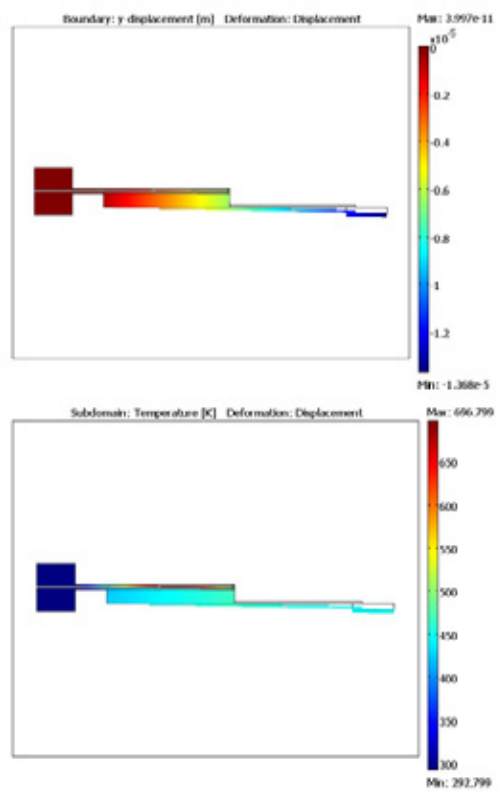

Figure 6: [top] An example of the displacement results of the large microactuator. [bottom] An example of the temperature profile of the microactuator under voltage.

4.2 Small Microactuator

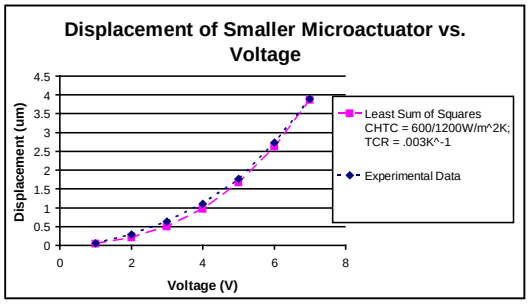

Figure 7: Results of the small microactuator. A best-fit sweep is plotted with the experimental displacement vs. voltage.

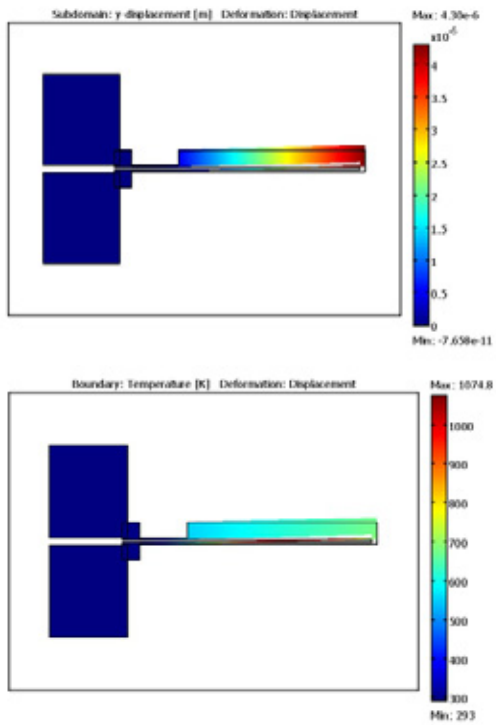

Figure 8: Results of the small microactuator. [top] The device clearly deflects toward the cold arm. [bottom] The extreme temperatures on the hot arm responsible for the actuation are apparent.

5. Conclusion and Future Work

The microactuators' sizes do cause changes in their thermal behavior; however, the expected results were that the smaller actuator would show a smaller Convective Heat Transfer Coefficient while the Temperature Coefficient of Resistivity would be very similar in both devices since they are made using the same SOIMUMPs process. The percent difference between their TCR's and their average is ±25%. Nevertheless, the TCR was positive and large for both, consistent with literature on the subject. The large CHTC of the smaller device and the dramatic difference between the two CHTC's is harder to explain but seems to be due, in terms of the small device, to the smaller trench and its closer proximity to the extreme heat of the hot arm. Surely, future work must be to establish thermal expansion as a function of temperature and n^{++} doping; then interpolated function(s) can be entered, perhaps modeling an anisotropic situation, as subdomain conditions. Also necessary is a more comprehensive look at heat loss as a function of size; in the future, an experiment with several actuators of different sizes will yield a trend perhaps. Finally, in lieu of the lack of research in the thermal expansion, a direct temperature measurement could omit the need for measuring displacement, an indirect way of measuring dramatically temperature dependent phenomena.

6. Acknowledgements

This work was funded with grants from NASA, Maine Space Grant Consortium and the University of Southern Maine.

7. References

[1] K. Miller, A. Cowen, G. Hames & B. Hardy, *SOIMUMPs design handbook, version 4.0*, Research Triangle Park, NC, MEMScAP, (2004) retrieved on March 31, 2009 from: http://www.memscap.com/en_mumps.html

[2] S. S. Li, *The dopant density and temperature dependence of electron mobility and resistivity in n-type silicon, Semiconductor measurement technology: NBS special publication 400 – 33* Washington, U.S. Department of Commerce/ National Bureau of Standards, (1977).

[3] H. M. Chuang, S. Tsai, K. Thei, & W. Liu, Anomalous temperature dependent characteristcs of silicon diffused resistors, *Electronics Letters*, 39, 1015–1016 (2003)

[4] G. Elert, *The Physics Factbook, Resistivity of gold*, (2009) Retrieved on March 31, 2008 from

http://hypertextbook.com/facts/2004/JennelleBaptiste.shtml

[5] T. C. Duc, G. Lau, J. F. Creemer, & P. M. Sarro, Electrothermal microgripper with large jaw displacement and itegrated force sensors, *Microelectromechanical Systems*, 17, 1546–1555 (2008)

[6] Q. Huang, & N. K. Lee, Analysis and design of polysilicon thermal flexure actuator, *Micromechanics and Microengineering*, 9, 64–70 (1999)

[7] J. Lee, C.M. Spadaccini, E.V. Mukerjee, & W.P. King, Differential scanning calorimeter based on suspended membrane single crystal silicon microhotplate, *Microelectromechanical Systems*, 17, 1513–1525 (2008)

[8] J. Lee, T. L. Wright, M. R. Abel, E. O. Sunden, A. Marchenkov, S. Graham, & W. P. King, Thermal conduction from microcantilever heaters in partial vacuum, *Applied Physics*, 101, [Note(s): 014906.1–014906.6] (2007)

[9] G. Sberveglieri, W. Hellmich, & G. Müller, Silicon hotplates for metal oxide gas sensor elements, *Microsystems Technologies*, 3, 183–190 (1997)

[10] A. A. Geisberger, N. Sarkar, M. Ellis, & G. D. Skidmore, Electrothermal properties and modeling of polysilicon microthermal actuators, *Microelectromechanical Systems*, 12, 513–523 (2003)

[11] S. Astie, A.M. Gue, E. Scheid, & J.P. Guillemet, Design of a Low Power SnO_2 Gas Sensor Integrated on Silicon oxynitride membrane, *Sensors and Actuators, B*, 67, 84 – 88, (2000)

[12] S. Astie, A.M. Gue, E. Scheid, L. Lescouzeres, & A. Cassagnes, Optimization of an integrated SnO_2 gas sensor using a FEM simulator, *Sensors and Actuators A*, 69, 205–211 (1998)

[13] A. Pike, & J. W. Gardner, Thermal modeling and characterisation of micropower chemoresistive silicon sensors, *Sensors and Actuators B*, 45, 19–26 (1997)

[14] N. Chronis, & L. P. Lee, Electrothermally activated SU-8 microgripper for single cell manipulation in solution, *Microelectro mechanical Systems*, 14, 857–863 (2005)

[15] D. T. W. Wong, P. C. H. Chan, L. Sheng, & J. K. O. Sin, Thermal modeling of micro-hotplates for integrated sensor applications, *Proc. IEEE Electron Devices Meeting*, Hong Kong, 149–152 (1997)

[16] N. D. Mankame, & G. K. Ananthasuresh, Comprehensive thermal modeling and characterization of an electro-thermal-compliant microactuator, *Micromechanics and Microengineering*, 11, 452–462 (2001)

[17] T. Moulton, & G. K. Ananthasuresh, Micromechanical devices with embedded electro-thermal-compliant actuation, *Sensors and Actuators A*, 90, 38–48 (2001)

[18] C. Tsamis, A. G. Nassiopoulou, & A. Tserepi, Thermal properties of suspended porous silicon micro-hotplates for sensor applications, *Sensors and Actuators B*, 95, 78–82 (2003)

[19] Efunda, *Thermal conductivity: silicon* Sunnyvale, CA, Efunda, (2009), Retrieved on July 11, 2009 from http://www.efunda.com/materials/elements/TC_Table.cfm?Element_ID=Si

[20] C. J. Glassbrenner, & G. A. Slack, Thermal conductivity of silicon and germanium from 3°K to the melting point, *Physical Review A*, 134, 1058–1069 (1964) as cited on the Ioffe Physical Technical Institute website at http://www.ioffe.rssi.ru/SVA/NSM/Semicond/Si/reference.html, on March 2, 2009.

[21] J. C. Thompson, & B. A. Younglove, *Physics and Chemistry of. Solids*, 20, 146–149, (1961) as cited on the Ioffe Physical Technical Institute website at http://www.ioffe.rssi.ru/SVA/NSM/Semicond/Si/Figs/ 15.gif on March 2, 2009.

[22] H. Watanabe, N. Yamada, M Okaji, Thermal expansion coefficient of silicon from 293–1000K, *International Journal of Thermophysics* , 25, 221–236 (2004)